All-Scalable $CH_3NH_3PbI_3$ Perovskite Solar Cells Fabricated in Ambient Air

Yameen Ahmed, Deepak Thrithamarassery Gangadharan, Mohammad Reza Kokaba, Vishal Yeddu, Muhammad Awais, Dongyang Zhang, Vahid Kamraninejad, and Makhsud I. Saidaminov

2023

Solar RRL
www.solar-rrl.com

All-Scalable $CH_3NH_3PbI_3$ Perovskite Solar Cells Fabricated in Ambient Air

Yameen Ahmed, Deepak Thrithamarassery Gangadharan, Mohammad Reza Kokaba, Vishal Yeddu, Muhammad Awais, Dongyang Zhang, Vahid Kamraninejad, and Makhsud I. Saidaminov**

Perovskite solar cells (PSCs) are an attractive emerging photovoltaic technology due to their high-performance while being made by low-cost fabrication processes. The most efficient PSCs are small area and made by nonscalable coating method in an inert atmosphere, but these sizes and fabrication conditions are commercially irrelevant. Herein, fabrication of PSCs is reported using only scalable methods, that is, slot-die coating and blade coating methods, all in ambient air. The tolerance to relaxed fabrication conditions is enabled by the use of hydrated nonhalogenated lead source. Resurfacing strategy is then introduced to suppress charge carrier nonradiative recombination and obtained an efficiency of 19.91% for rigid and 17.4% for flexible PSCs by all-scalable fabrication. To the best of our knowledge, these are the highest efficiencies for n–i–p structured $MAPbI_3$-based PSCs in ambient air using all-scalable method to date. The devices showed excellent tolerance to oxygen and moisture (ISOS-D-1) as well as stable maximum power point operation following burn in a dry air glove box (relative humidity ≈ 20%) without encapsulation.

1. Introduction

Perovskite solar cells (PSCs) have demonstrated an unprecedented surge in power conversion efficiency (PCE) over a decade of their development and reached a PCE of 25.8%, comparable to performance of matured silicon solar technology with a record PCE of 26.1% (after a research and development of ≈70 years).[1] The exceptional performance of PSCs is attributed to their outstanding optoelectronic properties such as long carrier diffusion length, high-light absorption coefficient ($\approx 10^5\ cm^{-1}$), tolerance to structural defects, tunable bandgap, and low-cost fabrication process.[2]

The most efficient PSCs are small-area devices ($\approx 0.1\ cm^2$) fabricated in an inert environment using spin coating method, but unfortunately these sizes and fabrication conditions are commercially irrelevant.[3] Spin coating produces inhomogeneous thin film over a large area disabling the manufacture of solar modules.[4] Inert atmosphere is neither sustainable environmentally nor favored by industry. Therefore, there is a growing demand for scalable fabrication of PSCs in relaxed manufacturing conditions. Researchers including us have demonstrated promising approaches for fabrication of small-area PSCs in ambient air;[5] it is now important to do just that, but for scalable fabrication strategies. Among scalable fabrication techniques (e.g., blade coating, slot-die coating, spray coating, and inkjet printing),[6] slot-die coating offers high reproducibility and industrial-scale adaptability,[7] as it can be directly applied for sheet-to-sheet and roll-to-roll processes.[8]

In this work, we report slot-die coated methylammonium lead iodide ($MAPbI_3$) thin film using dual-lead source precursor.[9] We then show fabrication of all-scalable PSCs by combining blade coating with slot-die coating. We then introduce isopropanol (IPA) washing step to induce excess lead iodide (PbI_2) at the grain boundaries and passivate the defects. We achieve a PCE of 20.87% for slot-die coated perovskite devices (where hole transport layer (HTL) and electron transport layer (ETL) were spin coated, and perovskite layer was slot-die coated; abbreviated as "slot-die coated" from here in the manuscript) and 19.91% and 17.4% for all-scalable (where HTL, ETL, and IPA were blade coated and perovskite layer was slot-die coated) rigid and flexible PSCs, respectively. To the best of our knowledge, these are the highest efficiencies for

Y. Ahmed, M. R. Kokaba, M. Awais, M. I. Saidaminov
Department of Electrical & Computer Engineering
University of Victoria
3800 Finnerty Road, Victoria, British Columbia V8P 5C2, Canada
E-mail: msaidaminov@uvic.ca

D. Thrithamarassery Gangadharan, V. Yeddu, D. Zhang, V. Kamraninejad, M. I. Saidaminov
Department of Chemistry
University of Victoria
3800 Finnerty Road, Victoria, British Columbia V8P 5C2, Canada
E-mail: deepaktg@uvic.ca

D. Thrithamarassery Gangadharan
Research and Development Division
Solaires Entreprises Inc.
2610 Douglas Street, Victoria, British Columbia V8T 4M1, Canada

M. I. Saidaminov
Centre for Advanced Materials and Related Technologies (CAMTEC)
University of Victoria
3800 Finnerty Road, Victoria, British Columbia V8P 5C2, Canada

The ORCID identification number(s) for the author(s) of this article can be found under https://doi.org/10.1002/solr.202300288.

DOI: 10.1002/solr.202300288

all-scalable n–i–p $MAPbI_3$-based PSCs in ambient air. Abate et al. showed a PCE of 21.44% for PSCs with slot-die coated perovskite layer, and spin-coated hole-transporter and passivation layers.[10]

2. Results and Discussion

2.1. Choice of Precursors

The nature of lead counter-ions plays a critical role in the crystallization and hence the morphology of perovskite films. In conventional spin coating fabrication of perovskite films, lead halide precursors are used in combination with an antisolvent (e.g., diethyl ether, chlorobenzene) treatment to produce dense, pinhole free perovskite films. In a scalable fabrication approach, however, antisolvent treatment is not compatible, but the use of lead halide salts without antisolvent leads to poor coverage of perovskite film (Figure S1, Supporting Information).

We hence turned our attention to lead acetate ($Pb(Ac)_2$) as a primary lead source in slot-die coating of perovskite film. $Pb(Ac)_2$ is known to offer a high rate of nucleation which enables compact pinhole free perovskite film without applying antisolvents.[11] In contrast, the rapid nucleation leaves no time for the growth of crystalline grains; thus formed small crystallites offer short charge carrier diffusion and inferior performing solar cells.[12] We added lead chloride ($PbCl_2$) into $Pb(Ac)_2$ precursor ink to balance nucleation versus growth aiming pinhole free and 500+ nm grain size (comparable to the thickness of perovskite film); the balance, we found, was at $Pb(Ac)_2$:$PbCl_2$ molar ratio of 8:1, twice larger than previously suggested (8:2) (Figure S2, Supporting Information).[9b]

For perovskite composition, we chose $MAPbI_3$ composition, as it requires low annealing temperature (≈100 °C) and can be applied on flexible substrates. We hence chose methylammonium iodide (MAI) as our methylamine (MA) source whose role is to provide enough halogen ion to build perovskite structure, as well as enough counter-ion (MA) to remove Ac and Cl

$$27MAI_{(solution)} + 8PbAc_{2(solution)} + PbCl_{2(solution)} \rightarrow 9MAPbI_{3(solid)} + 16MAAc^{\uparrow} + 2MACl^{\uparrow} \quad (1)$$

Slot-die coating of these precursor salts in a single solvent of N,N-dimethylformamide (DMF) in ambient air led to a mirror-like perovskite film (Movie S1, Supporting Information). In this refined perovskite ink, we posit, that the following factors aid in the ambient air fabrication of perovskite film. First, methylammonium acetate (MAAc), which, is formed in situ as a side product, aids in ambient air fabrication of PSCs.[5j,13] Second, the strong bond of Pb^{2+} with Ac^- in $PbAc_2$ reduces the density of under-coordinated Pb aids in ambient air fabrication.[14] Third, the use of $PbAc_2{\cdot}3H_2O$ instead of anhydrous $PbAc_2$ significantly improved the efficiency and reproducibility of PSCs (Figure S3, Supporting Information). Perovskite hydrate $MAPbI_3{\cdot}xH_2O$ which forms during the film processing hinders external water ingression enabling reproducible device in ambient condition.[15] The small amount of water in $PbAc_2{\cdot}3H_2O$ regulates the nucleation and crystal growth of perovskite films, but eventually leaves the reaction medium through evaporation[16]

$$27MAI_{(solution)} + 8PbAc_2{\cdot}3H_2O_{(solution)} + PbCl_{2(solution)} \rightarrow 9MAPbI_{3(solid)} + 16MAAc^{\uparrow} + 2MACl^{\uparrow} + 3H_2O^{\uparrow} \quad (2)$$

It is worth noting that the perovskite ink we developed is made of only four components ($PbAc_2{\cdot}3H_2O$, MAI, $PbCl_2$, and DMF) with no extra complexation or surfactant additives which are conventionally added into perovskite inks. Nevertheless, the ink is able to produce performing PSCs as we demonstrate below.

2.2. Film Resurfacing

When a nonhalide lead precursor like $Pb(Ac)_2{\cdot}3H_2O$ is used to produce $MAPbI_3$ films, an over-stoichiometric ratio of MA over lead precursor (3:1) is required as can be seen in the chemical Equation (1). The over-stoichiometric amount of MA can lead to the presence MA-based products (methylammonium chloride (MACl), MAAc) on the film. IPA can selectively wash off these,[17] as well as MAI from perovskite film forming surface PbI_2 which was shown to be beneficial for obtaining high efficiency PSCs.[18] Conventionally, excess PbI_2 is introduced by incorporation of nonstoichiometric addition of PbI_2 in the precursor solution. However, as we completely replaced PbI_2 with other lead sources in the precursor ink, we instead posited to obtain it on the surface by posttreatment. Excess PbI_2 on the surface and grain boundaries is beneficial as compared to that in the bulk of the perovskite film.[19] We note that lead-poor or lead-rich surfaces were addressed by chemical[20] and mechanical polishing in the past.[21]

We instead introduced IPA posttreatment to wash the perovskite surface in both slot-die coating and all-scalable methods. ^{1}Hydrogen nuclear magnetic resonance (^{1}H NMR) spectra of MAI in IPA shows MA resonance peak at 2.39 ppm; this peak is absent in pure IPA as expected, but it is present in the IPA solvent collected after the perovskite film treatment (**Figure 1**a). This confirms removal of MA-based reaction products from the surface.

X-Ray diffraction (XRD) of the perovskite films further confirms the formation of excess PbI_2 after IPA washing (Figure 1b). The diffraction intensity of the PbI_2 peak increased after IPA washing while that of perovskite remains unchanged. The PbI_2 to perovskite diffraction intensity ratio has increased from 0.0095 to 0.0124 after IPA washing step.

We observed, surprisingly, an improved surface coverage after the IPA treatment likely due partial surface rearrangement (Figure 1d,e). We observed that the density of cracks and pinholes has significantly decreased after IPA treatment (Figure 1e), while the density of brighter grains, which we attribute to PbI_2, also indicated by XRD (Figure 1b) has increased. Cross-sectional scanning electron microscope (SEM) images of the perovskite films with and without IPA washing step show excellent vertical grain alignment as a result of balanced nucleation and growth as discussed above (Figure 1f).

We then studied photophysical properties of the films before and after IPA washing. Perovskite film on bare glass with IPA washing showed an increased photoluminescence (PL) (Figure 1c-inset). Time resolved PL (TRPL) profiles (Figure 1c) exhibited bi-exponential decay kinetics: the fast decay component (τ_1) is attributed to the charge carrier trapping induced by trap states at surfaces and grain boundaries, while the slow decay

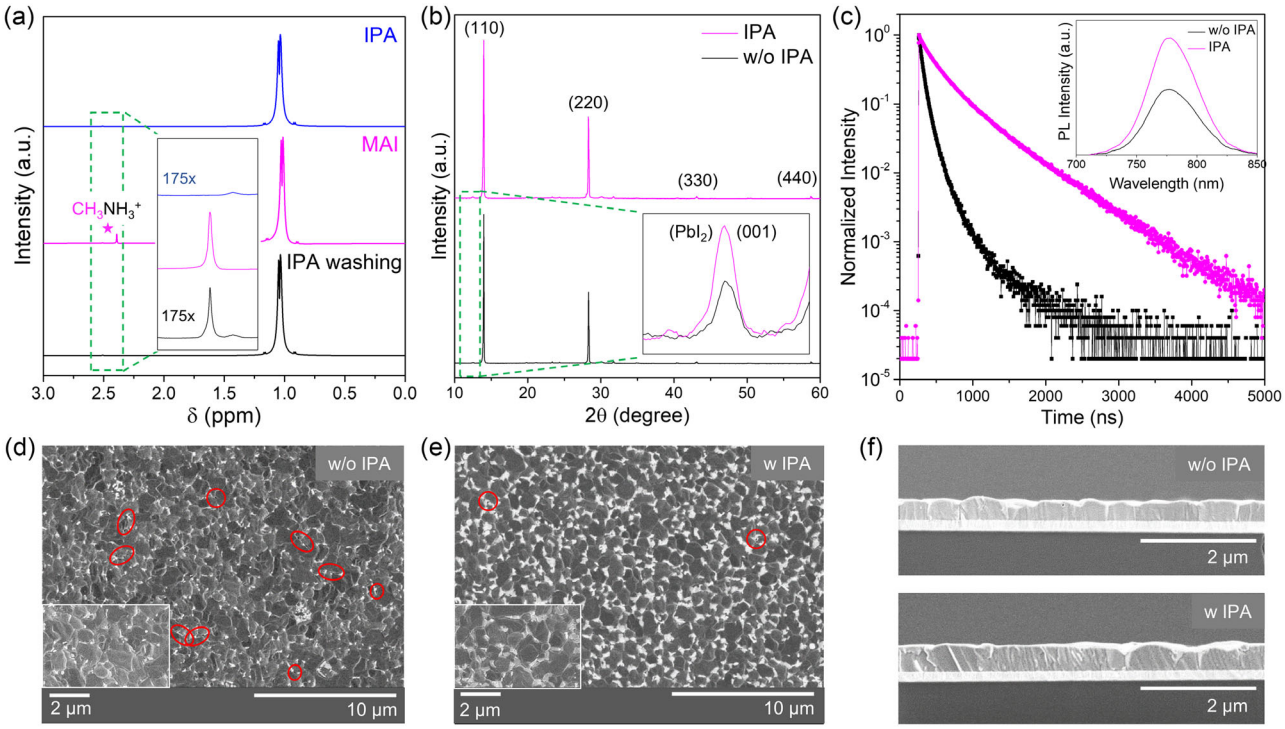

Figure 1. a) ^{1}HNMR spectra of IPA, MAI dissolved in IPA and sample-washed IPA. b) XRD spectra of perovskite films with and without IPA washing (inset shows PbI_2 peak). c) TRPL and PL (inset) spectra of perovskite films on bare glass. d,e) Surface SEM (red circles indicate pinholes while the red ovals——crack sat grain boundaries), and f) cross-sectional SEM of perovskite films on SnO_2 with and without IPA washing step.

component (τ_2)—to bulk radiative recombination (Table S1, Supporting Information).[22] Following IPA washing step, the films displayed a significant improvement in carrier lifetime from $\tau_1 = 38$ ns and $\tau_2 = 106$ ns to $\tau_1 = 143$ ns and $\tau_2 = 465$ ns, respectively, implying reduced nonradiative recombination.[23] PL spectra of the perovskite film on SnO_2 with and without IPA washing step are shown in Figure S4, Supporting Information. When using SnO_2 substrate instead (which we used as an electron transport layer in fabricating solar cells), the perovskite film showed prominent PL quenching after IPA washing, indicating enhanced charge transport/transfer between perovskite and SnO_2.

2.3. Solar Cells

Inspired by these observations, we fabricated planar n–i–p structured PSCs with a configuration of indium tin oxide (ITO)/tin (IV) oxide (SnO_2)/$MAPbI_3$/Spiro-OMeTAD/gold (Au), in which perovskite was deposited by slot-die coating method (**Figure 2**a). We obtained a champion PCE of 20.87% for slot-die coated perovskite layer (with IPA washing by spin coating) with a short circuit current density (J_{sc}), open circuit voltage (V_{oc}), and fill factor (FF) of 23.77 mA cm^{-2}, 1.06 V, and 82.6%, respectively (Figure 2b). To demonstrate the scalability of the fabrication process, we made devices only using scalable methods such as slot-die coating and blade coating methods (where perovskite layer was slot-die coated and, SnO_2, Spiro-OMeTAD, and IPA were blade coated) and obtained a champion PCE of 19.91% with a J_{sc}, V_{oc}, and FF of 23.36 mA cm^{-2}, 1.04 V, and 81.6%, respectively. To the best of our knowledge, this is the highest efficiency achieved so far for all-scalable n–i–p structure $MAPbI_3$-based PSCs where no spin coating is involved (Figure 2c, Table S2, Supporting Information). For PSCs prepared with all-scalable method without IPA washing, we obtained a champion PCE of 17.82% with a J_{sc}, V_{oc}, and FF of 21.72 mA cm^{-2}, 1.02 V, and 79.9%. The current voltage (J–V) curves of the champion devices for all-scalable method with and without IPA washing are shown in Figure 2b.

The J_{sc} obtained from integrating external quantum efficiency (EQE) and from JV characteristic showed a good agreement (Figure S5a, Supporting Information).[24] The devices showed no change in performance as a function of different scan rates (Figure S5b–d, Supporting Information). IPA-washed devices showed less hysteresis (9.5%) than the control devices (14.3%).

Figure 3 shows the performance of 55 PSCs with an active area of 0.049 cm^2 fabricated with all-scalable method with and without IPA washing. The results show clear increase of performance, largely due to V_{oc}, after IPA washing step.

For flexible PSCs fabricated with all-scalable method, we obtained a PCE of 17.4% with a J_{sc}, V_{oc}, and FF of 22.9 mA cm^{-2}, 1.02 V, and 74.4%, respectively. The J–V curve for champion flexible PSC is shown in Figure S6, Supporting Information.

To check the uniformity of the film with slot-die coating and all-scalable methods, we fabricated devices with different active area (**Figure 4**a-inset). The highest photovoltaic parameters of the PSCs with different active areas are shown in Figure 4a,b. We obtained PCEs of 15.28%, 15.28%, 18.11%, and 18.74% for active

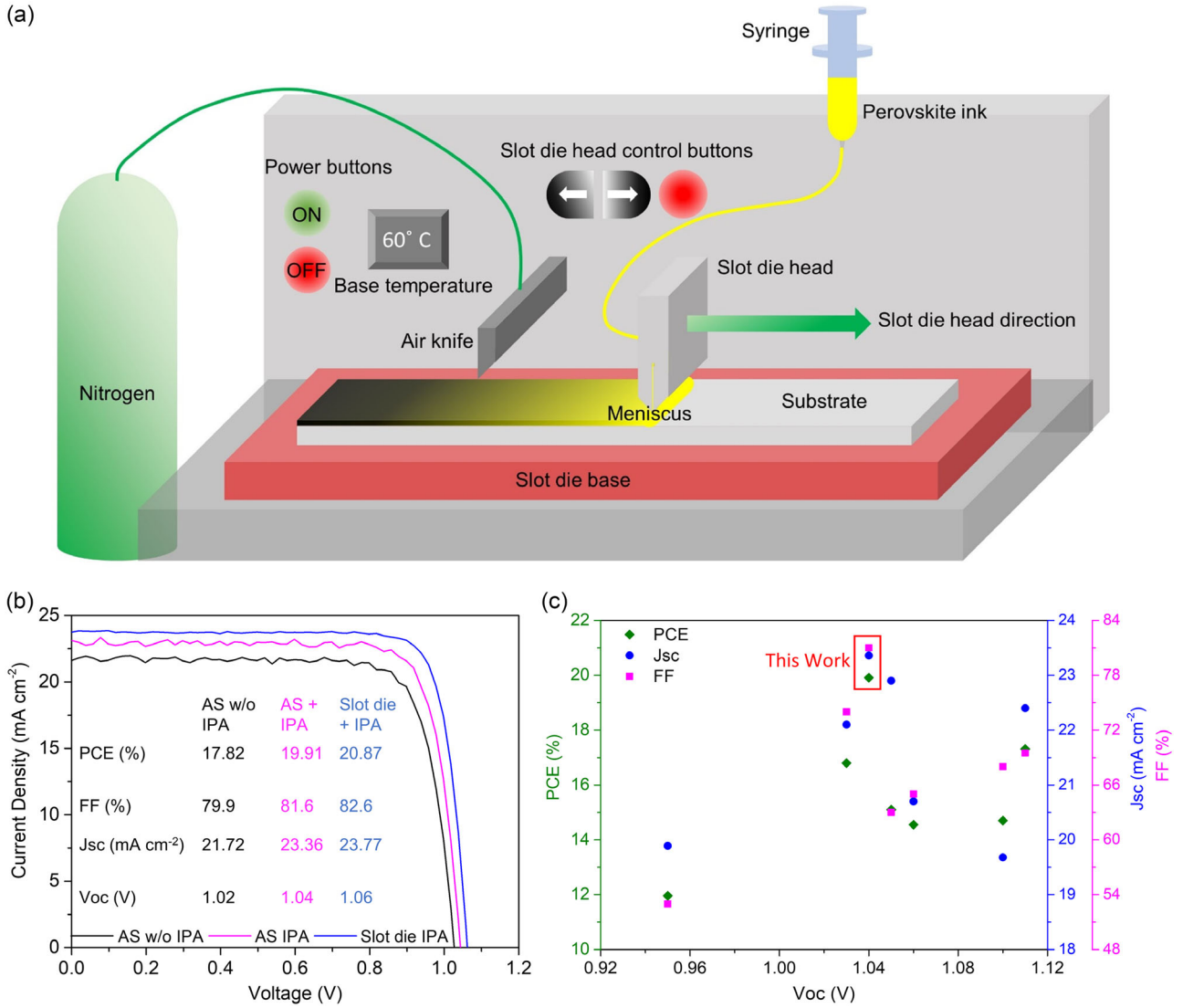

Figure 2. a) Schematic illustration of slot-die coating process. b) *J–V* curves of champion devices for slot-die and all-scalable (AS) methods. c) Summary of performance metrics achieved for all-scalable n–i–p structure $MAPbI_3$-based PSCs. Data points are taken from Table S2, Supporting Information.

areas of 1.03, 0.503, 0.189, and 0.049 cm^2, respectively. With increased devices area, FF loss becomes dominant which can be addressed by engineering conductivity of electrodes.

The PSCs showed excellent tolerance to oxygen and moisture (ISOS-D-1)[25] with negligible loss in fill factor when stored in ambient air with no encapsulation for 88 days (Figure S7, Supporting Information). The PSCs exhibited good operational stability under continuous illumination at maximum power point (MPP) for 100 h without encapsulation inside a dry air glove box (RH ≈ 20%) (Figure 4c). After burn-in period, the MPP of the IPA-washed device stabilized, even showing minor positive slope (Figure S8, Supporting Information). In contrast, the control PSC showed continuous negative PCE slope throughout the MPP test. We observed limited burn-in period in the control device, likely because its PCE has already dropped to ≈12%.

3. Conclusion

We demonstrated $MAPbI_3$ PSCs fabricated by scalable methods (i.e., slot-die coating and all scalable) in ambient air from non-halide lead source. We showed that washing perovskite surface with IPA significantly improved the performance of PSCs due to the defect passivation. As a result, we reported nearly 20% for all-scalable n–i–p $MAPbI_3$ devices, the highest for fully scalable fabrication of $MAPbI_3$ to date. We also obtained a PCE of 17.4% for flexible PSCs using all-scalable method. Future works should focus on fabricating $PbAc_2$-based formamidinium lead iodide ($FAPbI_3$) PSCs, as this composition shows highest efficiencies reported to date. Earlier attempts demonstrated that simply replacing MAI with FAI led to formation of nonperovskite phase due to aminolysis. This has been recently addressed by the use of ammonia to form mixed cation (FACs)-based PSCs from $PbAc_2$

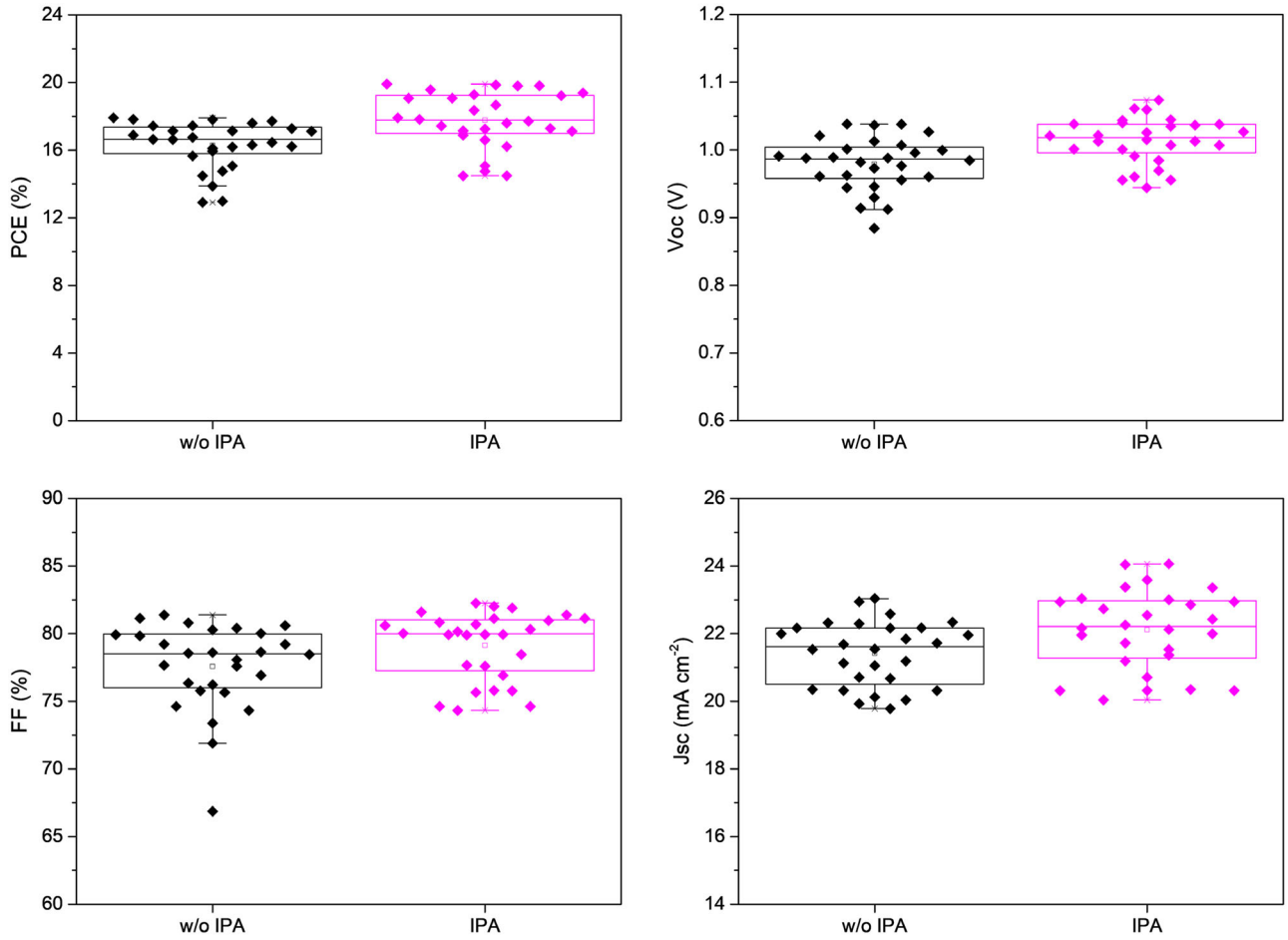

Figure 3. Statistical data of PSCs fabrication with all scalable with and without IPA washing step. The boxes indicate the 25th and 75th percentiles. The whiskers indicate the 5th and 95th percentiles. The median and mean are represented by the line dividing the boxes and the open square symbols, respectively. The cross symbols represent the maximum and minimum values.

precursor.[26] We envision that the similar strategy can be applied to make $FAPbI_3$ PSCs.

4. Experimental Section

Materials: ITO coated glass substrates were purchased from Shang Yang Solar (X07-10 A). Tin (IV) oxide (SnO_2) 15% in H_2O colloidal dispersion solution, lead acetate trihydrate ($PbAc_2{\cdot}3H_2O$, 99.995%), and lead chloride ($PbCl_2$, 99%) were purchased from the Alfa Aesar. Methylammonium iodide (MAI, >99.99%) was purchased from Great Cell. N, N-dimethyl formamide (DMF, 99.5%), chlorobenzene (99.5%), and acetonitrile (ACN, ≥99.9%) solvents were parched from Milipore Sigma. Cobalt salt (FK 209 Co(III) TFSI), 4-tert-Butylpyridine (tBP, 98%), and bis (trifluoromethane) sulfonimide lithium salt (Li-TFSI 99.95%) were purchased from Milipore Sigma. Sprio-OMeTAD was purchased from Xi'an Polymer Light Technology Co., Ltd.

Preparation of Perovskite Precursor Solution: The $MAPbI_3$ perovskite precursor solution was prepared by dissolving MAI and PbX_2 (where X = Ac, Cl) in 3:1 ratio, and $PbAc_2$:$PbCl_2$ in 8:1 ratio dissolved in DMF to make 0.75 M solution.

Preparation of Spiro-OMeTAD: Spiro-OMeTAD (0.1 g) was dissolved in chlorobenzene (1.1 mL). Additionally, 23 µL of Li-TFSI solution (520 mg mL^{-1} in acetonitrile), 39 µL of tBP and 10 µL of FK 209 Co(III) TFSI solution (375 mg mL^{-1} in acetonitrile) was mixed in the Spiro solution and filtered it before use.

Device Fabrication: Patterned 3.25 × 7.5 cm glass/ITO substrates were cleaned successively with deionized water, acetone, and IPA by sonication for 15 min each and dried them in oven. The cleaned substrates were then ozone treated for 15 min before depositing the SnO_2 layer. For slot-die coating method, ETL, and HTL were deposited by spin coating method while for all-scalable method, ETL and HTL were deposited by blade coating method.

For Spin Coated Electron Transport Layer: SnO_2 colloidal solution diluted with deionized water was spin coated at 3000 rpm for 30 s followed by annealing at 150 °C for 30 min.[5e]

For Blade Coated Electron Transport Layer: SnO_2 solution was drop cast in the middle of the ITO substrate and blade coated on a heated substrate. The SnO_2 coated substrates were then transferred to the hot plate for annealing at 150 °C for 30 min.

Slot-die coater was used for the deposition of perovskite layer for both slot-die and all-scalable methods. The SnO_2 coated substrates were treated with UV ozone for 15 min before depositing the perovskite layer. The perovskite precursor solution was coated onto the SnO_2 layer at a coating speed of 15 mm s^{-1} with a gap of ≈100 µm between the substrate and the meniscus. The solution feed was maintained at 0.5 mL s^{-1} with a syringe pump, and a continuous nitrogen flow was supplied at a speed of 10 m s^{-1}. The base heat of the slot-die coater was set to 60 °C before the

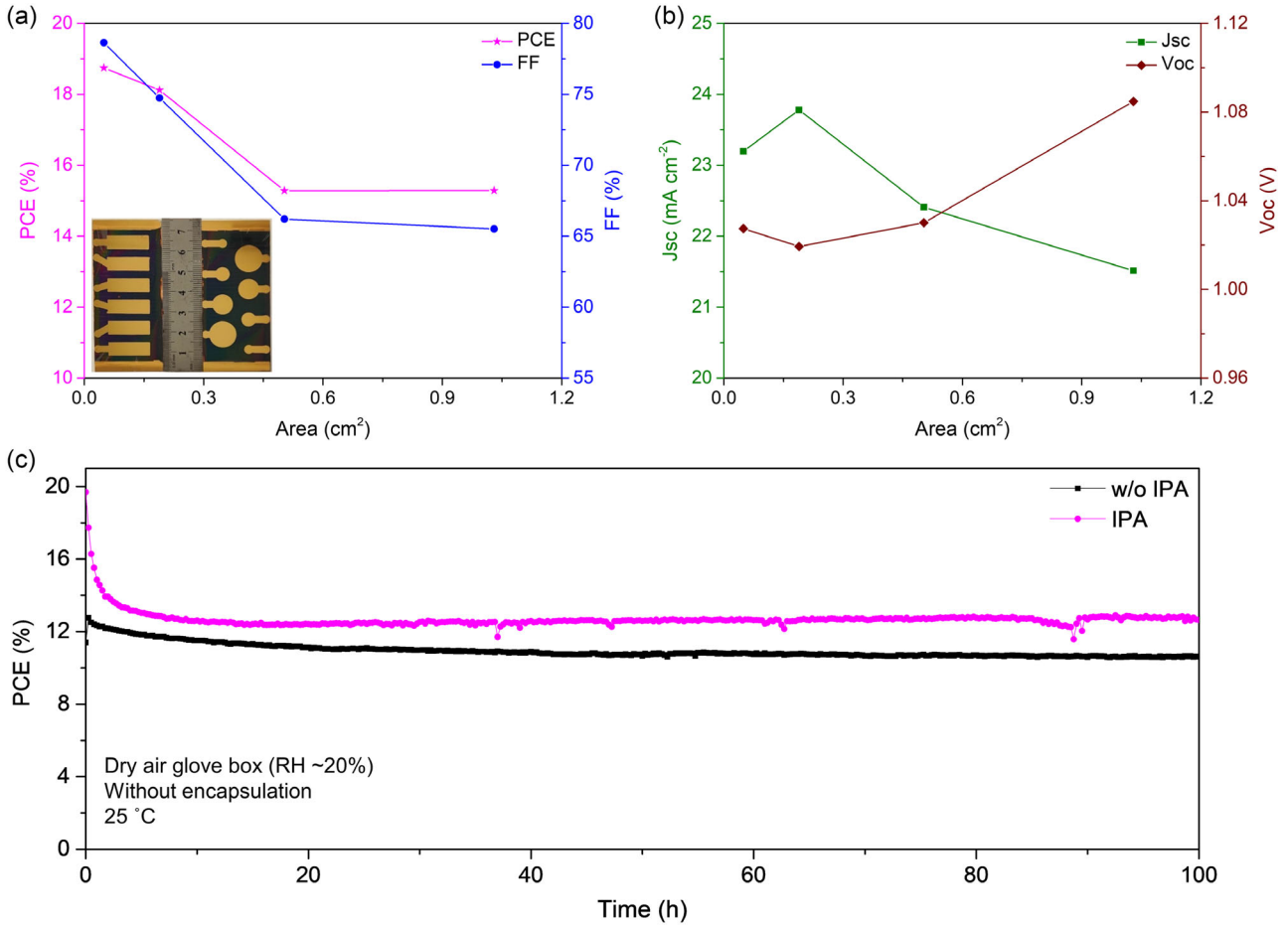

Figure 4. a,b) Photovoltaic parameters for different active area devices, (a-inset). Photograph of PSCs with different active area pixels and 1 cm^2, c) Maximum power point tracking in a dry box without encapsulation at 25 °C.

perovskite deposition. Perovskite coated substrate was thermally annealed at 100 °C for 10 min. For flexible devices, the base heat was increased to 70 °C and annealing temperature was set to 140 °C. 3.25 × 7.5 cm polyethylene terephthalate (PET) flexible substrates with ITO and a sheet resistance of 15 Ω sq^{-1} was used. Due to the large size of these substrates, they curved making it challenging to anneal. We then sticked the substrate on a screen protector to flatten them. This led to ≈35 °C difference between hot plate displayed temperature and the actual temperature on the surface. Therefore, we increased the hot plate displayed temperature to 140 °C, thus reaching actual 100 °C on the substrate.

The perovskite films were washed with IPA by spin coating for slot-die coating method and blade coated for all scalable and annealed them at 100 °C for 10 min.

For Spin Coated Isopropanol Washing: IPA washing step was performed by dropping 400 µL of IPA on the rotating perovskite film at a rotation speed of 3000 rpm per second for 30 s.

For Blade Coated Isopropanol: 50 µL of IPA was drop casted on the perovskite film and blade coated at between the perovskite film and the blade.

For Spin Coated Hole Transport Layer: Spiro-OMeTAD solution was spin coated dynamically onto the perovskite film at a speed of 2000 rpm for 30 s.

For Blade Coated Hole Transport Layer: 50 µL of Spiro-OMeTAD solution was drop cast on the perovskite film and blade coated at a heated substrate.

All the above-mentioned steps were performed in ambient air.

Last, 80 nm gold electrodes were deposited by thermal evaporation under vacuum at 10^{-6} Torr.

Characterization: PSCs were fabricated in the air. XRD measurements were done with a PANalytical Empyrean system using a Cu (Kα, 1.5406 Å) source. SEM images were obtained with a Hitachi S-4800 field emission SEM. PL spectroscopy was carried out by UV–Vis AVENTES spectrometer (AvaSpec-ULS2048CL-EVO-RS) in the reflection mode ranging from 500 to 780 nm in a dark room every 2 s. TRPL measurement were performed on an Edinburgh Instruments OB920 Single Photon Counting system. The samples were excited using a 510 nm pulsed laser diode. Emission was collected at 780 nm using a 16 nm bandwidth monochromator. ^{1}H NMR spectra were acquired with a Bruker AVANCE-III Neo 500 MHz spectrometer. Photovoltaic parameters were measured with Newport Oriel sol-3 A (class AAA) solar simulator at standard 1.5 a.m. solar irradiance, and data were recorded with Ossila source meter by scanning the cell from 1.2 to −0.100 V. Similarly, for operational stability measurements, PSCs were placed in a custom-designed LED simulator, and data were recorded with Ossila source meter with time interval of 15 min between each measurement. EQE measurements were performed with PTS-1-SR (Sciencetech Inc.).

Supporting Information

Supporting Information is available from the Wiley Online Library or from the author.

Acknowledgements

Y.A. and D.T.G. contributed equally to this work. The authors thank Solaires Entreprises Inc. and Canada's Natural Sciences and Engineering Research Council (ALLRP 561355-20) for their financial support. M.I.S. is grateful to the NSERC (RGPIN-2020-04239), the Canadian Foundation for Innovation and B.C. Knowledge Development Fund (40326), and the Canada Research Chairs Program (CRC-2019-00297) for financial support.

Conflict of Interest

The authors declare no conflict of interest.

Data Availability Statement

The data that support the findings of this study are available from the corresponding author upon reasonable request.

Keywords

ambient air, flexibility, scalable coating, slot-die coating, surface passivation

Received: April 18, 2023
Revised: May 25, 2023
Published online: June 16, 2023

[1] a) R. S. Ohl, *US Patent 2443542*, **1941**; b) M. A. Green, *Prog. Photovolt.: Res. Appl.* **2009**, *17*, 183; c) NREL.

[2] a) B. Chen, S.-W. Baek, Y. Hou, E. Aydin, M. De Bastiani, B. Scheffel, A. Proppe, Z. Huang, M. Wei, Y.-K. Wang, *Nat. Commun.* **2020**, *11*, 1257; b) Y. Ahmed, B. Khan, M. B. Faheem, K. Huang, Y. Gao, J. Yang, *J. Energy Chem.* **2022**, *67*, 361; c) Z. Yang, M. Wei, O. Voznyy, P. Todorovic, M. Liu, R. Quintero-Bermudez, P. Chen, J. Z. Fan, A. H. Proppe, L. N. Quan, G. Walters, H. Tan, J. W. Chang, U. S. Jeng, S. O. Kelley, E. H. Sargent, *J. Am. Chem. Soc.* **2019**, *141*, 8296; d) J. Kim, G. Kim, T. K. Kim, S. Kwon, H. Back, J. Lee, S. H. Lee, H. Kang, K. Lee, *J. Mater. Chem. A* **2014**, *2*, 17291; e) J. Yang, B. D. Siempelkamp, D. Liu, T. L. Kelly, *ACS Nano* **2015**, *9*, 1955; f) Y. Hou, E. Aydin, M. De Bastiani, C. Xiao, F. H. Isikgor, D.-J. Xue, B. Chen, H. Chen, B. Bahrami, A. H. Chowdhury, *Science* **2020**, *367*, 1135.

[3] a) Y. Rong, Y. Hu, A. Mei, H. Tan, M. I. Saidaminov, S. I. Seok, M. D. McGehee, E. H. Sargent, H. Han, *Science* **2018**, *361*, eaat8235; b) A. Verma, D. Martineau, E. Hack, M. Makha, E. Turner, F. Nuesch, J. Heier, *J. Mater. Chem. C* **2020**, *8*, 6124; c) H. Tan, A. Jain, O. Voznyy, X. Lan, F. P. Garcia de Arquer, J. Z. Fan, R. Quintero-Bermudez, M. Yuan, B. Zhang, Y. Zhao, F. Fan, P. Li, L. N. Quan, Y. Zhao, Z. H. Lu, Z. Yang, S. Hoogland, E. H. Sargent, *Science* **2017**, *355*, 722.

[4] a) J. H. Heo, F. Zhang, C. Xiao, S. J. Heo, J. K. Park, J. J. Berry, K. Zhu, S. H. Im, *Joule* **2021**, *5*, 481; b) D.-K. Lee, N.-G. Park, *Sol. RRL* **2022**, *6*, 2100455.

[5] a) K. Jung, K. Oh, J. W. Choi, K. C. Kim, M.-J. Lee, *Nano Energy* **2021**, *89*, 106387; b) J. Wu, J. J. Dong, S. X. Chen, H. Y. Hao, J. Xing, H. Liu, *Nanoscale Res. Lett.* **2018**, *13*, 293; c) X. J. Wang, X. Q. Ran, X. T. Liu, H. Gu, S. W. Zuo, W. Hui, H. Lu, B. Sun, X. Y. Gao, J. Zhang, Y. D. Xia, Y. H. Chen, W. Huang, *Angew. Chem. Int. Ed.* **2020**, *59*, 13354; d) R. Xia, X. X. Gao, Y. Zhang, N. Drigo, V. I. E. Queloz, F. F. Tirani, R. Scopelliti, Z. J. Huang, X. D. Fang, S. Kinge, Z. F. Fei, C. Roldan-Carmona, M. K. Nazeeruddin, P. J. Dyson, *Adv. Mater.* **2020**, *32*, 2003801; e) M. Awais, D. T. Gangadharan, F. Tan, M. I. Saidaminov, *Chem. Mater.* **2022**, *34*, 8112; f) J. Wang, L. Yuan, H. Luo, C. Duan, B. Zhou, Q. Wen, K. Yan, *J. Chem. Eng.* **2022**, 136968; g) M. Wang, H. Sun, L. Meng, M. Wang, L. Li, *Adv. Mater.* **2022**, 2200041; h) Z. Wang, J. J. Jin, Y. P. Zheng, X. Zhang, Z. K. Zhu, Y. Zhou, X. X. Cui, J. H. Li, M. H. Shang, X. Z. Zhao, S. Liu, Q. D. Tai, *Adv. Energy Mater.* **2021**, *11*, 2102169; i) K. M. Salim, S. Masi, A. F. Gualdrón-Reyes, R. S. Sánchez, E. M. Barea, M. Krečmarová, J. F. Sánchez-Royo, I. Mora-Seró, *ACS Energy Lett.* **2021**, *6*, 3511; j) L. Chao, Y. Xia, X. Duan, Y. Wang, C. Ran, T. Niu, L. Gu, D. Li, J. Hu, X. Gao, *Joule* **2022**, *6*, 2203; k) G. L. Wang, Q. Lian, D. Wang, F. Jiang, G. J. Mi, D. Y. Li, Y. L. Huang, Y. Wang, X. Y. Yao, R. Shi, C. Liao, J. H. Zheng, A. Ho-Baillie, A. Amini, B. M. Xu, C. Cheng, *Adv. Mater.* **2022**, *34*, 2205143; l) M. Wang, H. X. Sun, M. Wang, L. Li, *Nano Today* **2022**, *42*, 101371; m) L. Zhang, X. Z. Zhang, Y. Yu, X. X. Xu, J. Tang, X. He, J. H. Wu, Z. Lan, *Sol. Energy* **2017**, *155*, 942; n) M. I. Saidaminov, J. Kim, A. Jain, R. Quintero-Bermudez, H. R. Tan, G. K. Long, F. R. Tan, A. Johnston, Y. C. Zhao, O. Voznyy, E. H. Sargent, *Nat. Energy* **2018**, *3*, 648; o) W. Hui, L. Chao, H. Lu, F. Xia, Q. Wei, Z. Su, T. Niu, L. Tao, B. Du, D. Li, *Science* **2021**, *371*, 1359.

[6] a) L. Vesce, M. Stefanelli, J. P. Herterich, L. A. Castriotta, M. Kohlstadt, U. Wurfel, A. Di Carlo, *Sol. RRL* **2021**, *5*, 2100073; b) D. S. Ham, W. J. Choi, H. Yun, M. Kim, D.-H. Yeo, S. Lee, B. J. Kim, J. H. Lee, *ACS Appl. Energy Mater.* **2021**, *4*, 7611; c) E. Berger, M. Bagheri, S. Asgari, J. Zhou, M. Kokkonen, P. Talebi, J. Luo, A. F. Nogueira, T. Watson, S. G. Hashmi, **2022**, *6*, 2879; d) X. Dai, S. Chen, H. Jiao, L. Zhao, K. Wang, Z. Ni, Z. Yu, B. Chen, Y. Gao, J. Huang, *Nat. Energy* **2022**, *7*, 923; e) L.-H. Chou, J. M. Chan, C.-L. Liu, *Sol. RRL* **2022**, *6*, 2101035.

[7] a) R. Patidar, D. Burkitt, K. Hooper, D. Richards, T. Watson, *Mater. Today Commun.* **2020**, *22*, 100808; b) M. B. Faheem, B. Khan, J. Z. Hashmi, A. Baniya, W. Subhani, R. S. Bobba, A. Yildiz, Q. Qiao, *Cell Rep. Phys. Sci.* **2022**, 100827; c) H. Li, X. Feng, K. Huang, S. Lu, X. Wang, E. Feng, J. Chang, C. Long, Y. Gao, Z. Chen, *Small* **2023**, 2300374.

[8] a) P. Liu, G. Tang, F. Yan, *Sol. RRL* **2022**, *6*, 2100683; b) K. K. Sears, M. Fievez, M. Gao, H. C. Weerasinghe, C. D. Easton, D. Vak, *Sol. RRL* **2017**, *1*, 1700059.

[9] a) D. Lee, Y.-S. Jung, Y.-J. Heo, S. Lee, K. Hwang, Y.-J. Jeon, J.-E. Kim, J. Park, G. Y. Jung, D.-Y. Kim, *ACS Appl. Mater. Interfaces* **2018**, *10*, 16133; b) W. Qiu, T. Merckx, M. Jaysankar, C. M. de la Huerta, L. Rakocevic, W. Zhang, U. W. Paetzold, R. Gehlhaar, L. Froyen, J. Poortmans, D. Cheyns, H. J. Snaith, P. Heremans, *Energy Environ. Sci.* **2016**, *9*, 484.

[10] S. Y. Abate, Z. Yang, S. Jha, G. Ma, Z. Ouyang, H. Zhang, S. Muhammad, N. Pradhan, X. Gu, D. Patton, *Chem. Eng. J.* **2023**, *457*, 141199.

[11] a) D. T. Moore, H. Sai, K. W. Tan, D.-M. Smilgies, W. Zhang, H. J. Snaith, U. Wiesner, L. A. Estroff, *J. Am. Chem. Soc.* **2015**, *137*, 2350; b) W. Zhang, M. Saliba, D. T. Moore, S. K. Pathak, M. T. Hörantner, T. Stergiopoulos, S. D. Stranks, G. E. Eperon, J. A. Alexander-Webber, A. Abate, *Nat. Commun.* **2015**, *6*, 6142.

[12] S. Venkatesan, F. Hao, J. Y. Kim, Y. G. Rong, Z. Zhu, Y. L. Liang, J. M. Bao, Y. Yao, *Nano Res.* **2017**, *10*, 1413.

[13] L. Chao, Y. Xia, B. Li, G. Xing, Y. Chen, W. Huang, *Chem* **2019**, *5*, 995.

[14] Y. Zhang, Y. Ma, I. Shin, Y. K. Jung, B. R. Lee, S. Wu, J. H. Jeong, B. H. Lee, J. H. Kim, K. H. Kim, S. H. Park, *ACS Appl. Mater. Interfaces* **2020**, *12*, 7186.

[15] a) C. X. Ran, Y. Wang, W. Y. Gao, Y. D. Xia, Y. H. Chen, W. Huang, *Sol. RRL* **2021**, *5*, 2100665; b) C.-H. Chiang, C.-G. Wu, *ACS Nano* **2018**, *12*, 10355; c) D. Liu, C. J. Traverse, P. Chen, M. Elinski, C. Yang, L. Wang, M. Young, R. R. Lunt, *Adv. Sci.* **2018**, *5*, 1700484.
[16] W. Kong, G. Wang, J. Zheng, H. Hu, H. Chen, Y. Li, M. Hu, X. Zhou, C. Liu, B. N. Chandrashekar, *Sol. RRL* **2018**, *2*, 1700214.
[17] L. Y. Zheng, L. N. Shen, U. C. Yilmazoglu, T. Zhu, D. Zhang, J. Zheng, X. Gong, *Org. Electron.* **2022**, *111*, 106653.
[18] a) Q. Chen, H. Zhou, T.-B. Song, S. Luo, Z. Hong, H.-S. Duan, L. Dou, Y. Liu, Y. Yang, *Nano Lett.* **2014**, *14*, 4158; b) Z. Ma, D. Huang, Q. Liu, G. Yan, Z. Xiao, D. Chen, J. Zhao, Y. Xiang, C. Peng, H. Li, *J. Energy Chem.* **2022**, *66*, 152; c) D.-K. Lee, D.-N. Jeong, T. K. Ahn, N.-G. Park, *ACS Energy Lett.* **2019**, *4*, 2393.
[19] a) L. He, H. Su, Z. Li, H. Liu, W. Shen, *Adv. Funct. Mater.* **2023**, 2213963; b) A. Merdasa, A. Kiligaridis, C. Rehermann, M. Abdi-Jaleb, J. Stober, B. Louis, M. Gerhard, S. D. Stranks, E. L. Unger, I. G. Scheblykin, *ACS Energy Lett.* **2019**, *4*, 1370.
[20] a) L. Zhao, Q. Li, C.-H. Hou, S. Li, X. Yang, J. Wu, S. Zhang, Q. Hu, Y. Wang, Y. Zhang, *J. Am. Chem. Soc.* **2022**, *144*, 1700; b) S. Fu, J. Le, X. Guo, N. Sun, W. Zhang, W. Song, J. Fang, *Adv. Mater.* **2022**, *34*, 2205066.
[21] a) Y. Lin, Y. Liu, S. Chen, S. Wang, Z. Ni, C. H. Van Brackle, S. Yang, J. Zhao, Z. Yu, X. Dai, *Energy Environ. Sci.* **2021**, *14*, 1563; b) S. Chen, Y. Liu, X. Xiao, Z. Yu, Y. Deng, X. Dai, Z. Ni, J. Huang, *Joule* **2020**, *4*, 2661.
[22] a) Q. He, M. Worku, L. Xu, C. Zhou, S. Lteif, J. B. Schlenoff, B. Ma, *J. Mater. Chem. A* **2020**, *8*, 2039; b) J. W. Lee, Z. Dai, T. H. Han, C. Choi, S. Y. Chang, S. J. Lee, N. De Marco, H. Zhao, P. Sun, Y. Huang, Y. Yang, *Nat. Commun.* **2018**, *9*, 3021.
[23] D. H. Cao, C. C. Stoumpos, C. D. Malliakas, M. J. Katz, O. K. Farha, J. T. Hupp, M. G. Kanatzidis, *APL Mater.* **2014**, *2*, 091101.
[24] M. Saliba, L. Etgar, *ACS Energy Lett.* **2020**, *5*, 2886.
[25] M. V. Khenkin, E. A. Katz, A. Abate, G. Bardizza, J. J. Berry, C. Brabec, F. Brunetti, V. Bulović, Q. Burlingame, A. Di Carlo, *Nat. Energy* **2020**, *5*, 35.
[26] a) D. Luo, L. Zhao, J. Wu, Q. Hu, Y. Zhang, Z. Xu, Y. Liu, T. Liu, K. Chen, W. Yang, *Adv. Mater.* **2017**, *29*, 1604758; b) J. Zhao, S. O. Fürer, D. P. McMeekin, Q. Lin, P. Lv, J. Ma, W. L. Tan, C. Wang, B. Tan, A. S. Chesman, *Energy Environ. Sci.* **2023**; c) E. G. Moloney, D. T. Gangadharan, V. Yeddu, D. Zhang, S. Moradi, A. M. Askar, M. M. Adachi, D. C. Leitch, M. I. Saidaminov, *Chem. Mater.* **2022**, *34*, 4394.